

PREDICTION OF AXIAL THRUST LOAD ACTING ON A CRYOGENIC LIQUID TURBINE IMPELLER

Ke Wang; Jinju Sun^{*}; Zhilong He; Peng Song

School of Energy and Power Engineering, Xi'an Jiaotong Univ.,
No.28, Xianning West Road, Xi'an, Shaanxi, 710049, P.R. China

ABSTRACT

A single stage cryogenic liquid turbine is developed for replacing the Joule-Thompson valve and recovering energy from the liquefied air during throttling process in the large-scale internal compression air-separation unit, and evaluation of the impeller axial thrust at different conditions is essential for a reliable bearing design and stable operation. To predict the axial thrust load, a numerical model is established to simulate the turbine flow in a turbine stage environment, which includes the main flow domain (an asymmetrical volute, variable geometry nozzle, impeller, and diffuser), impeller front and back side gaps, and shaft seal leakage. Numerical simulation of flow is conducted by using the ANSYS-CFX. Flow characteristics in both main flow domain and impeller side gaps of the turbine stage are captured and analyzed. The axial thrust is then calculated based on the obtained pressure data in the impeller and its front and side gaps by using a direct integration approach.

Flow behaviour in both main flow domain and impeller side gaps has been well exhibited by the numerical results. At the impeller back side gap inlet, the back flow is encountered even for design condition and it returns the impeller main flow stream; the impeller side gap flow has much influence on the axial thrust. To investigate influence of turbine operation condition on axial thrust, flow simulation is conducted at different mass flow rates and inlet pressure for the turbine stage, based on which the axial thrust is calculated. It is demonstrated from the obtained numerical results that the axial thrust increases as the inlet pressure increases and decreases as turbine flow rate increases. Geometry parametric study is conducted for the shaft seal clearances, which has demonstrated that the axial thrust is influenced largely by the clearance size and it decreases as the clearance grows.

For the purpose of comparison, the empirical method is also used to predict the axial thrust load. The obtained results

are compared to the numerical ones and evident deviation of the empirical from the numerical exists and the reason is that axial force components caused by the impeller main flow stream and its side gap flow are approximated very roughly in the empirical method.

1. INTRODUCTION

In various cryogenic liquefaction cycle systems, such as air-separation, hydrocarbon processing, and LNG production units, cryogenic liquid turbines can be used to replace Joule-Thomson valves for energy saving purpose. In these processes, liquefied gases are often need to be throttled to satisfy the successive technological processes, and traditionally this is done by means of the J-T valve, which can cause considerable pressure head loss, and such wasted energy raise the temperature of the cryogenic unit leading to evaporation of liquefied gases and even cavitation damage to the structure. The use of liquid turbine is one of the most promising alternatives for throttling liquefied gas [1]. For example, in a LNG processing train, annual plant revenues can be increased by 3%-4% by using a pair of cryogenic liquid turbines [2], and in an internal compression air-separation unit, the total power consumption for oxygen production has been reduced by 3.1% with a liquid turbine [3].

In the development of liquid turbine, it is important to accurately predict the axial thrust load, since an appropriate axial thrust can ensure the mechanical reliability of the operational turbine [4-5]. An excessively large axial thrust load can cause various problems, such as bearing bush burnout, and seal diaphragm damage, and it can also cause the axial displacement of the impeller and main shaft leading to mechanical collision and failure. In addition, a large axial thrust requires oversized bearings, and subsequently increases the turbine size and manufacture cost. On the other hand, an

^{*} Contact author: Dr Jinju SUN, jjsun@mail.xjtu.edu.cn

excessively small axial thrust can lead to the axial drifting of the rotor and deteriorate its mechanical reliability. A use of undersized bearings can also cause mechanical failure. A good prediction of the axial thrust is much essential for a stable operation of the turbine.

The axial thrust of the turbine is associated with the main flow stream in impeller and gap flow in the front and back sides of the impeller, and influence of both flow behavior must be considered properly in the prediction of the thrust. There are mainly three types of methods used for predicting the axial thrust: the empirical, analytical and numerical approaches. For example, in references [6] and [7], the empirical method is proposed respectively for single stage and multi-stage centrifugal pumps with open, semi-open, and closed impellers. In reference [8], the analytical method is developed based on the flow analysis in the gap between rotating and stationary walls and it is used to predict the axial thrust for a rocket engine turbopump.

In recent years, with the rapid development and advances of Computational Fluid Dynamics (CFD) technology, numerical prediction of axial thrust based on CFD are reported by some investigators [9-16]. For example, Han and Cizmas use a numerical algorithm to predict the axial thrust of a centrifugal compressor. The flow filed within the impeller flow domain and the leakage gap on the back side of the impeller are investigated, and it is found that the leakage flow in impeller back side gap is asymmetrical. At some circumferential locations of leakage gap inlet, part of the leakage flow returns the impeller passage. This demonstrates that the impeller flow and the impeller back side flow interact largely and they must be solved as whole to model the real flow physics in the impeller and leakage flow. [10]. Della Gatta et al. predict the axial thrust of a multistage centrifugal pump through separated CFD analysis (3D simulation for the impeller flow filed and 2D analysis for the impeller chambers) [11]. Gantar et al. predicted the hydraulic axial thrust by using numerical method and experimental investigation in multistage pumps [12].

Previous work as mentioned above demonstrates that the CFD based numerical method is an effective way to predict the axial thrust, but some different approximations have been used in these studies to simplify the flow model and simulation, which can cause a large error in the subsequent prediction of the axial thrust. For example, the impeller side gap geometry is often treated by approximation, and the influence of labyrinth seal leakage flow on axial thrust load is rarely considered. The impeller flow and /or the gap flow are simulated separately without consideration of the interaction between adjacent components, rather than in a turbine stage environment. Moreover, in reference [11] and [16], the 3D flow simulation is conducted for the impeller, and the simplified 2D simulation used for gap flows, which is also biased from the real 3D flow characteristics in both impeller and gaps. Clearly there is yet still much to do in numerical prediction of axial thrust.

The objective of present study is to predict the axial thrust properly. A numerical model is established to simulate the turbine flow in a turbine stage environment, which includes the main flow domain (an asymmetrical volute, variable geometry nozzle, impeller, and diffuser), impeller front and back side

gaps, and shaft seal leakage. Numerical simulation of flow is conducted by using the ANSYS-CFX. Flow characteristics in both main flow domain and impeller side gaps of the turbine stage are captured and analyzed. The axial thrust is then calculated based on the obtained pressure data in the impeller and its front and side gaps by using a direct integration approach. Geometry parametric study on the axial thrust load is also carried out numerically, and influence of the seal clearance sizes is clarified. Additionally, for the purpose of comparison, the empirical method is also used to predict the axial thrust load and its deviation from the former is highlighted.

2. NUMERICAL METHOD AND SIMULATION

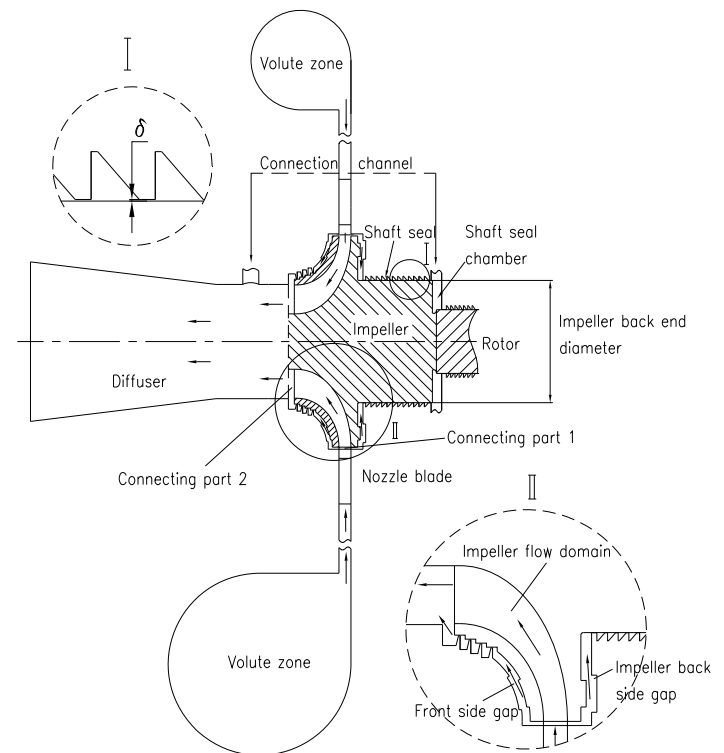


Figure 1 CROSSSECTION SKETCH OF LIQUID TURBINE

Flow Simulation

Physical model. The CFD simulation was carried out in a turbine stage environment using ANSYS-CFX software. The physical model for simulation consists of the asymmetrical volute, vaned nozzle, shrouded impeller, diffuser, impeller front and back side gaps, and shaft seal leakage, figure 1.

Grid. ANSYS-ICEM software is used to generate the grid for volute and leakage gaps. The unstructured grids are used for discretizing the volute zone with the mesh refinement at near wall and tongue region. The structured grids are generated for the seal leakage gaps. The geometry of vaned nozzle and shrouded impeller are reproduced by the CFX-Bladegen and the structured multi-block grids are generated by CFX-Turbogrid with an H/J/C/L and J grid topology. Figure 2 shows the computational grid of the turbine stage used in flow

simulation. Total size of the grid is 3795757, and the individual grid size for each component is given in table 1.

Table 1 GRID SIZE OF EACH COMPONENT

volute	nozzle	impeller	front side gap	back side gap	diffuser	connecting part 1	connecting part 2
661817	967200	1224000	268680	475320	102900	55520	40320

The grid quality was checked by using ICEM software and the good qualities of the grid have been reached, since the indicator of the grid quality is 0.3 above the recommended minimum value in help manual [17], and the minimum face angle of orthogonality is larger than 25 degrees. The y_+ for the entire turbine stage grid is less than 10.2, where it is 2.5 for the impeller mesh. The Reynolds number of the impeller is about 3.4×10^7 , and that of cavities is about 2.2×10^7 .

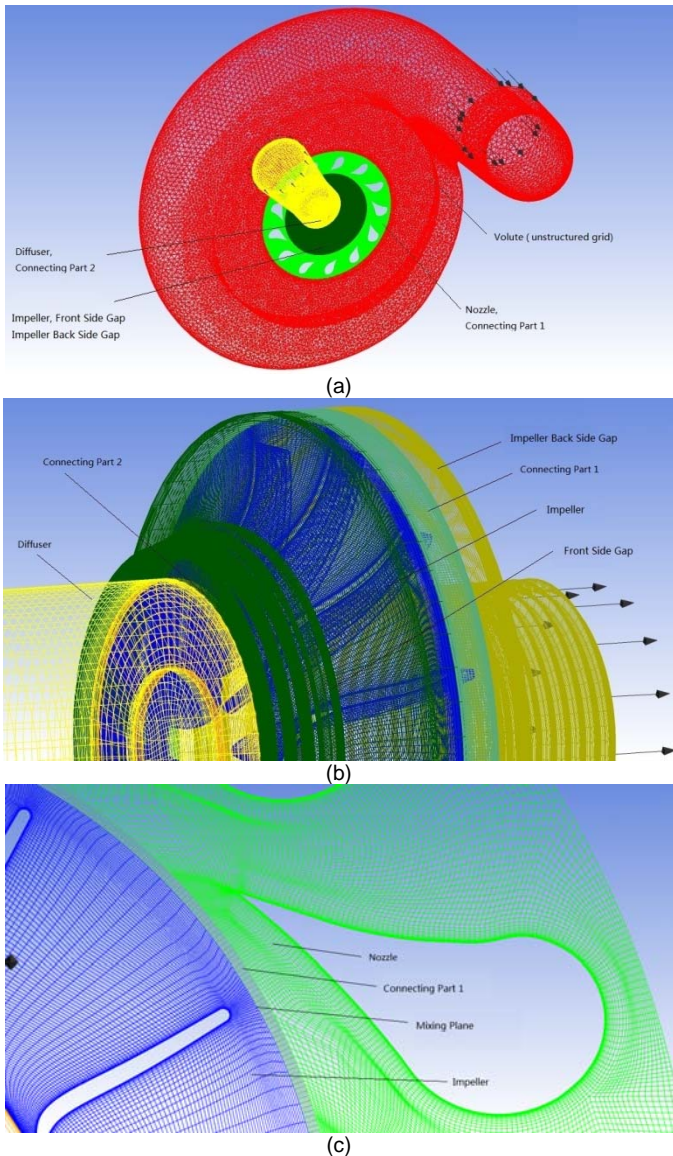


Figure 2 COMPUTATIONAL GRID OF THE TURBINE STAGE

To verify whether flow solution is grid independent or not, grid dependency studies are conducted to determine a fairly suited grid size for the simulation. The initial grid is 2.38 million, and then three larger grids are obtained through the refinement, i.e. 2.72 million, 3.80 million, and 4.5 million. The grids are refined especially at the near wall regions, such as end wall, and leading (LE) and trailing (TE) edge of the nozzle and impeller blades, and grid refinement is also carried out particularly around tongue region of the volute.

Flow simulation is carried out respectively for the four grids and accordingly the axial thrust and flow rate are predicted, which are compared in figure 3. When the predicted mass flow rate closes to the prescribed turbine flow rate and the RMS residual value reaches $1e-4$, the simulation is thought to be converged. It is demonstrated that the calculated axial thrust and mass flow rate change negligibly with a larger than 3.80 million grid, thus such a grid is justified and used in the present study.

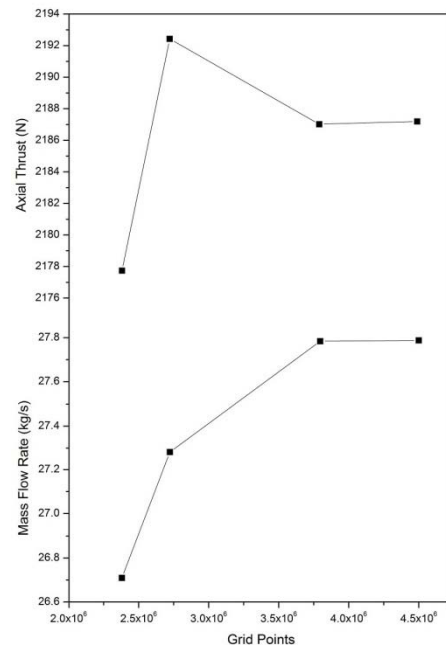


Figure 3 VARIATION OF CALCULATED AXIAL THRUST AND MASS FLOW RATE WITH GRID SIZE

Solver. The solver of ANSYS-CFX utilizes a control volume method based on finite volume discretization scheme to solve the unsteady Navier-Stokes equations in their conservation form with so-called coupled algebraic multigrid technology [18]. The total energy equation in CFX is used in the turbine simulation, and it includes the transport of enthalpy and also the kinetic energy effects. A coupled solver is applied to solve the hydrodynamic equations (for velocity components u , v , and w , and pressure p) as a single system. The steady flow models are used in the present study. As recommended by the CFX guide, the K-epsilon and shear stress transport models can be an alternative for modeling turbulent flow in liquid pumps and turbines. In CFX, the k-epsilon turbulence model uses the scalable wall-function approach to improve its robustness and

accuracy. The scalable wall functions allow for solution on arbitrarily fine near wall grids, which is a significant improvement over standard wall functions [18]. So, the $k-\epsilon$ turbulence model is adopted.

Properties of the liquefied air (such as dynamic viscosity, density and thermal conductivity) are not available in CFX-pre library materials, thus they are defined by using CEL (CFX Expression Language), and all the data used are output from the NIST REFPROP software.

Boundary condition. Total pressure (7 Mpa) and total temperature (97.19 K) are imposed at the turbine inlet boundary, and at the outlet boundary the static pressure (0.58 Mpa) is used. A mixing plane technique has been applied to the rotor-stator interfaces, and it performs a circumferential averaging of the fluxes through bands on the interface [18]. And the General Grid Interface (GGI) algorithm of CFX is used to define the domain interface. Then, steady state solutions are obtained in each reference frame.

Axial Thrust Calculation

As shown in figure 4, to determine the total axial thrust, each component force in the axial direction must be obtained. The total axial thrust acting on the impeller is expressed by

$$F = F_2 + F_4 - F_1 - F_0 - F_3 \quad (1)$$

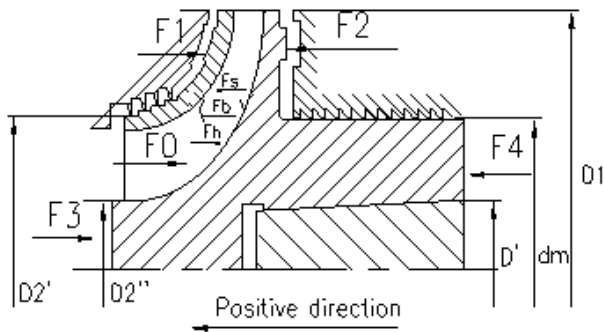


Figure 4 DIMENSIONS AND AXIAL FORCES OF IMPELLER

Where F_2 is the global force acting on the back side surface of the impeller, while F_1 on the front side; F_0 is the fluid-induced axial resultant force acting on the impeller inner surface. F_3 is pressure force due to the outlet pressure acting on the impeller outlet head face. F_4 is pressure force acting on the impeller back annular area, and pressure herein can be taken the same as the impeller outlet pressure, since the outlet of the shaft seal chamber is connected to the diffuser by a channel (as shown in figure 1). A use of such a structure is mainly to decrease the seal chamber outlet back pressure and achieve a better seal effect. Thus, outlet pressure of the shaft seal chamber remains constant to that of diffuser due to channel connection. Then F_4 can be readily calculated. The axial

thrust is then calculated based on the obtained pressure distributions by using a direct integration approach.

In the numerical procedure, force F_0 is obtained by a summation of the component forces acting on the impeller inner surfaces (i.e. the shroud, hub and blade surfaces), denoted respectively as F_s , F_h , and F_b , written as

$$F_0 = F_h - F_s - F_b \quad (2)$$

From the above analysis, to calculate the axial thrust properly, prediction of pressure distribution at both impeller front and back side gaps are also very important, which requires a real environment modeling of the gap flow physics. Specifications and dimensions of the shaft labyrinth seal are given respectively in table 2 and figure 5.

Table 2 DIMENSIONS AND CONDITIONS

Impeller back end diameter	24 mm
Clearance at teeth	0.05 mm
No. of teeth	11
Rotation speed	20000rpm
Outlet pressure	0.58Mpa
Fluid	Liquefied Air

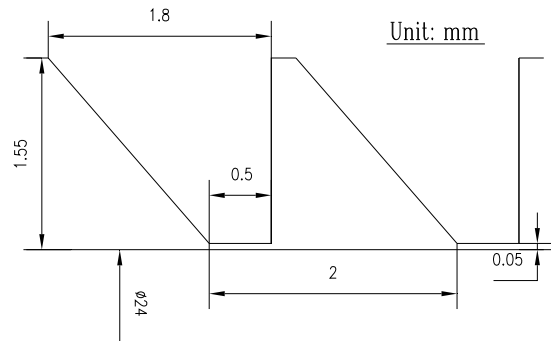


Figure 5 DIMENSIONS OF SHAFT SEAL

Figure 6 shows the labyrinth seal models used for the present study, and grids of impeller side gaps are shown in figure 7.

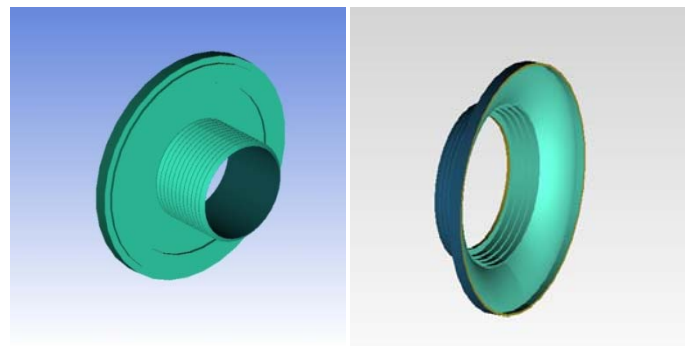


Figure 6 ANALYSIS MODEL FOR IMPELLER SIDE GAPS

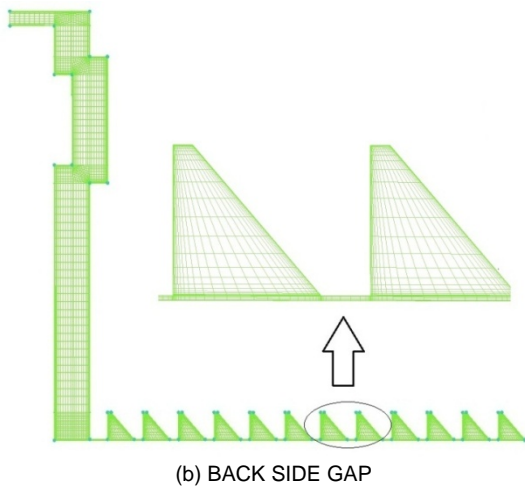
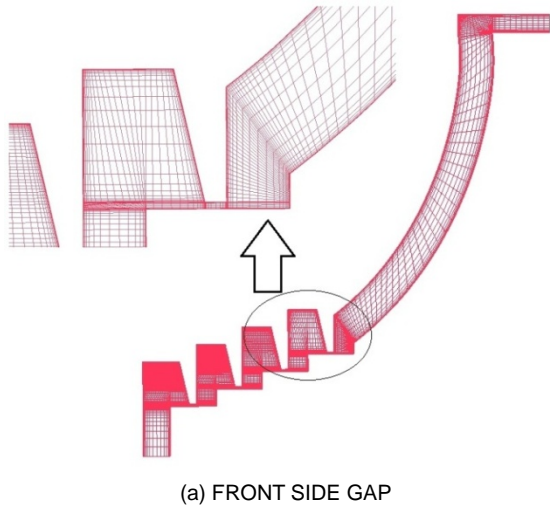


Figure 7 GRIDS OF IMPELLER SIDE GAPS

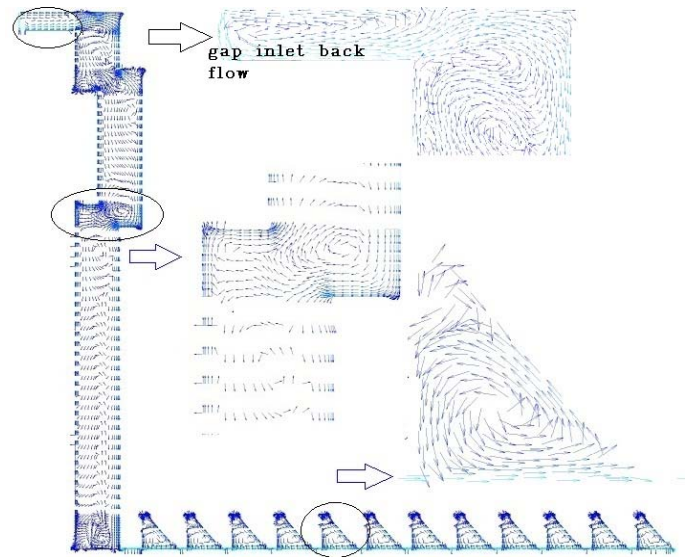


Figure 8 BACK SIDE GAP VELOCITY VECTOR

Figure 9 presents the pressure distribution in both front and back side gaps of impeller. The y^+ for front side gap grid is less than 10.2, and for impeller side gap grid is less than 9.3. Moreover, the wall normal growth ratios of grid have been all set to 1.2.

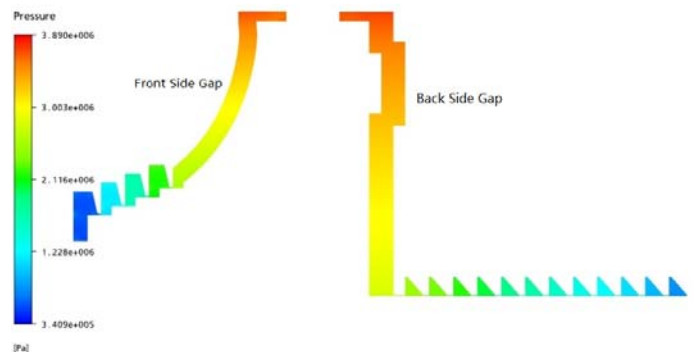


Figure 9 PRESSURE DISTRIBUTION IN IMPELLER SIDE GAPS

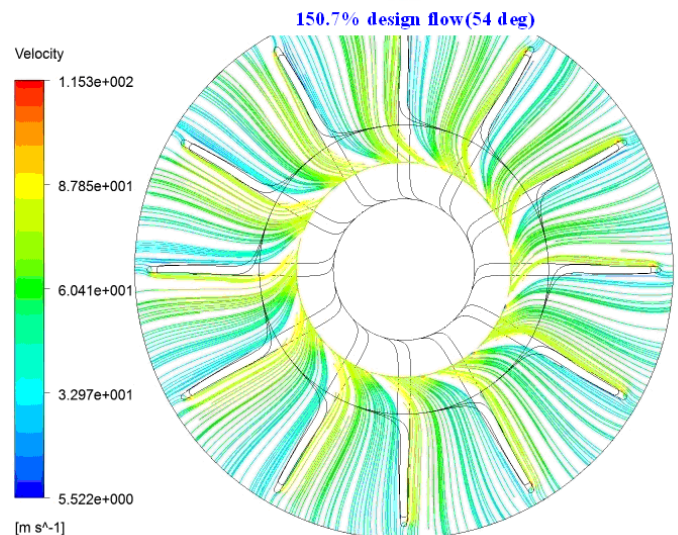
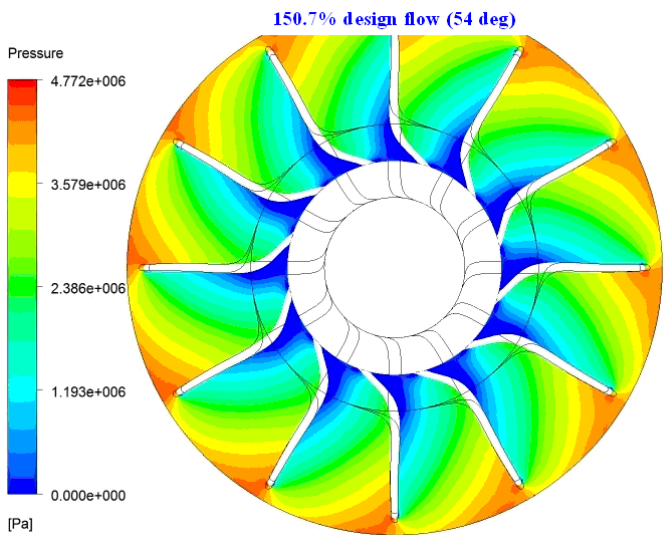
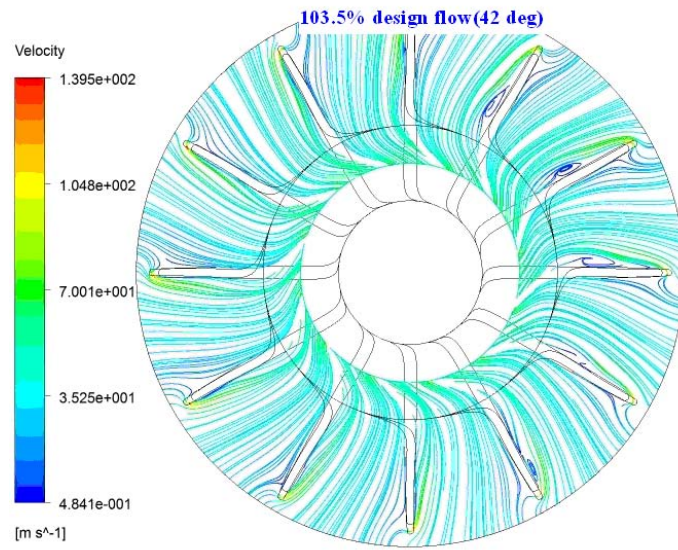
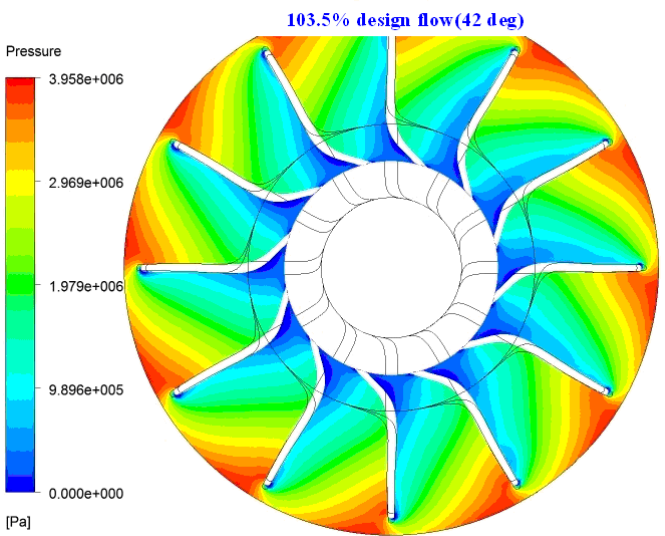
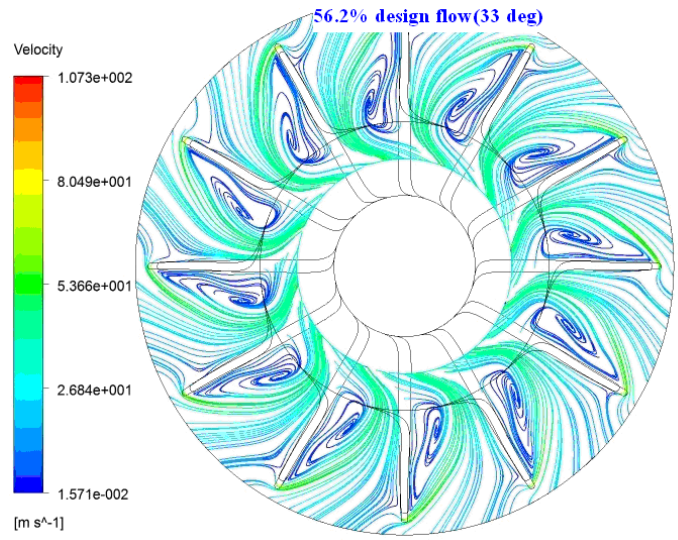
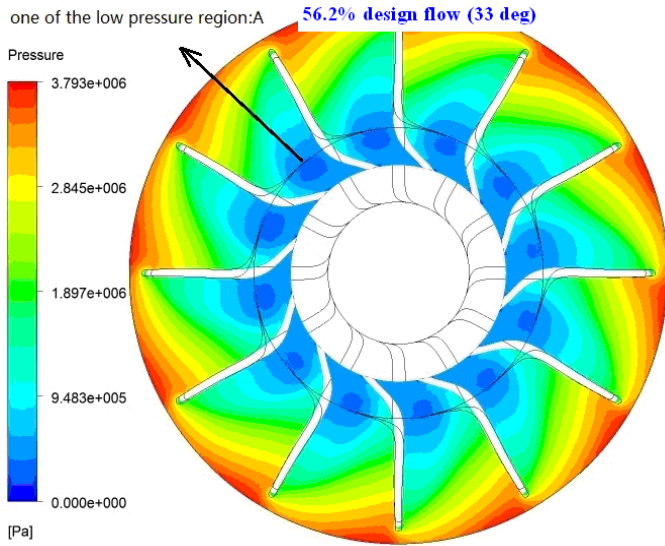
3. NUMERICAL RESULTS

Results from CFD simulation are much helpful to understand the flow physics in the small dimension flow regions, such as the impeller side gaps and shaft seal chambers. Figure 8 shows the predicted velocity vectors of the leakage flow in the impeller back side gaps and shaft seal chamber at design condition. A high speed jet at the tip of each tooth and a large vortex in the chamber are captured and at back side gap inlet, reversal of the leakage flow is apparent, the zoomed-in view in figure 8, which indicates some of back side gap leakage flow has returned the impeller main flow stream over a percentage gap inlet circumference.

With a 2D approximated model, the gap flow is often presumably taken as asymmetric; clearly such a model is unlikely to capture flow physics of gap inlet back flow.

Influence of Mass Flow Rate

To investigate the variations of axial thrust with different operating conditions, flow simulations are performed over a wide flow range (56.2%-151% design flow), which is realized by changing the nozzle vane setting.



(a) STATIC PRESSURE

(b) SURFACE STREAMLINE

Figure 10 STATIC PRESSURE AND SURFACE STREAMLINE AT DIFFERENT FLOW RATES (50% SPAN)

Flow behaviour is influenced largely by the turbine operation conditions and figure 10 compares the impeller flow at different flow rates, which corresponding to different nozzle vane stagger settings. As shown in figure 10(a), at 56.2% design flow, evident low pressure region is exhibited on the suction side of each impeller blade and it occupies rather large part of the blade passage space, which is caused by flow separation on the suction side as shown in figure 10(b), and a large scale separating vortex is produced on the suction side leading to pressure head dissipation, and subsequently a low pressure region. As the flow rate increases, the low pressure region becomes smaller and smaller, as shown by the pressure contours of 103.5%, and 150.7% design flow in figure 10 (a), and correspondingly the separating vortex becomes smaller at 103.5% and even invisible at 150.7% design flow.

Figure 11 presents the predicted axial thrust with mass flow rate. The axial thrust decreases from 2407.29 N to 1767.38 N, as the mass flow rate changes from 56.2%-151% design flow. Figure 12 presents the pressure variation with radius in the impeller back side gap at different flow rates and the pressure force acting on the back side of the impeller. The pressure distribution does not change evidently from 56.2% to 103.5% design flow, figure 12 (a), and there is no evident variation in F_2 within this flow range, figure 12(b). This corresponds to the axial thrust curve, as shown in figure 11, where the curve becomes relatively flat in this flow range. It shows that in this range the mass flow has not a significant effect on axial thrust. At flow rates above 120% design flow, F_2 increases rapidly, while the axial thrust decreases correspondingly. It is demonstrated that the impeller gap flow influence the axial thrust largely.

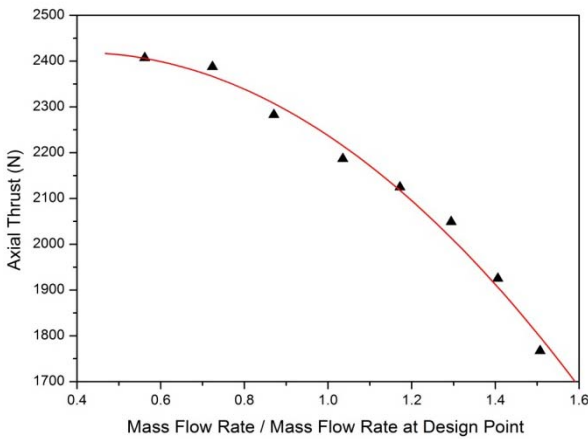
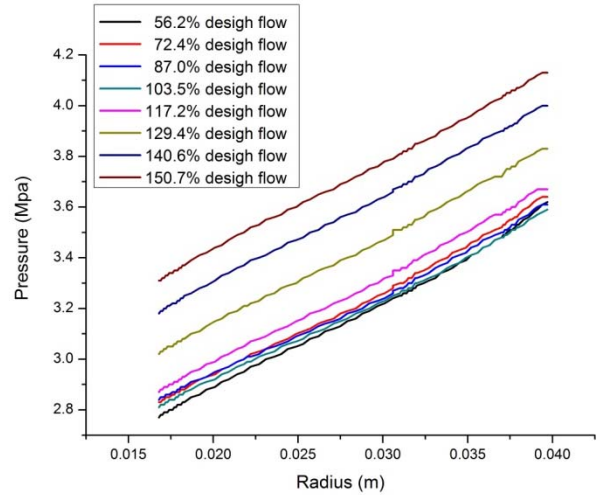
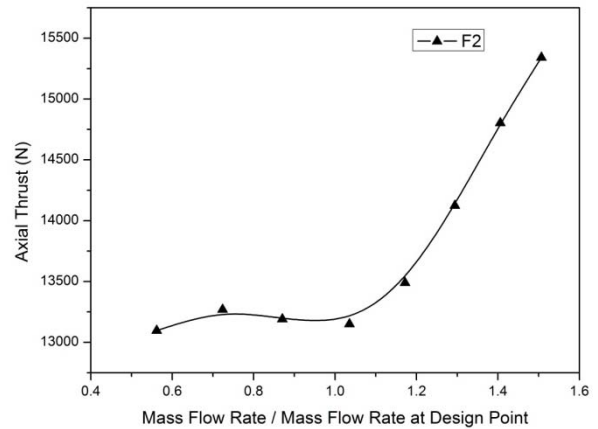


Figure 11 AXIAL THRUST AND MASS FLOW RATE



(a) PRESSURE DISTRIBUTION



(b) F_2

Figure 12 PRESSURE DISTRIBUTION AND AXIAL FORCE ON IMPELLER BACK SIDE

Velocity in impeller back side gap consists of mainly the tangential components and varies along the radial direction. Figure 13 presents the velocity profile at a section being 1.5mm offset from the rotating wall in the impeller back side gap at three different flow rates. Similar profiles are obtained for three different flow rates, and the gaps of three curves are visible but they are very small. It seems that the gap flow velocity is not influenced largely by the main flow rate. The reason may be that the rotating speed of rotor is large and the centrifugal force plays a dominant role in the flow physics in this gap region.

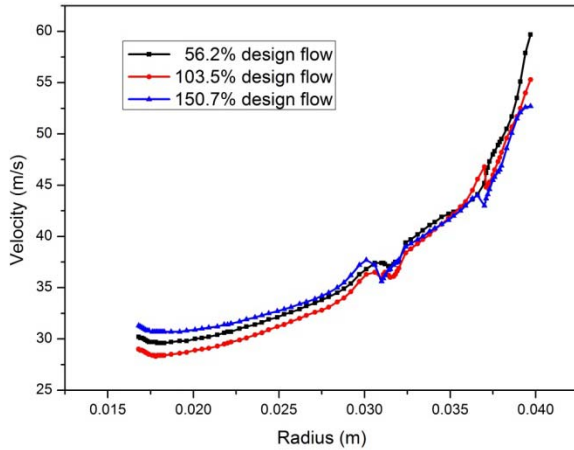


Figure 13 VELOCITY IN IMPELLER BACK SIDE GAP

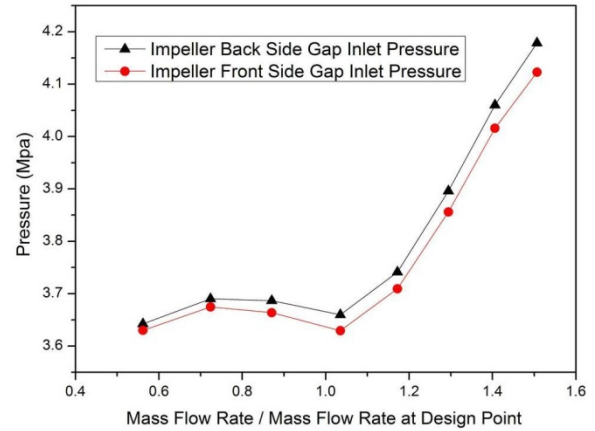


Figure 15 IMPELLER SIDE GAPS INLET PRESSURE AT DIFFERENT MASS FLOW RATE

Flow behavior in the turbine stage changes with the flow rate, and this brings about a change in axial forces, subsequently a change in axial thrust. Such variations of axial force and thrust with flow rate are predicted based on flow simulation. Figure 14 presents the component axial force variation with the flow rate. It is clear that F_1 and F_2 changes in accordance with each other and both increase evidently at large flow rates, thus $F_2 - F_1$ increases slowly. F_0 also increases evidently at large flow rate. As shown in figure 14, there is a small increase in resultant force $F_2 - F_1$ and force F_0 from 56.2% to 103.5% design flow, but the increase in resultant force $F_2 - F_1$ is smaller than that of F_0 . The axial thrust is expressed by equation 1, i.e. $F = F_2 + F_4 - F_1 - F_0 - F_3$, where force F_3 and F_4 held constant as being described in paragraph Axial Thrust Calculation. Based on the above analysis and equation 1, we can deduce that the axial thrust decreases with flow rates, which is also demonstrated by the CFD results presented in figure 11.

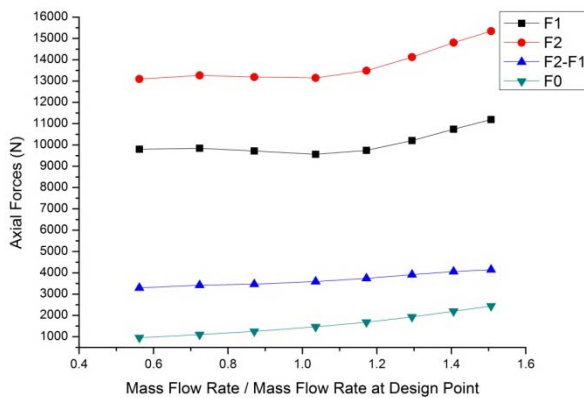


Figure 14 AXIAL FORCES VERSUS MASS FLOW RATE

Impeller side gap inlet pressure is influenced by turbine flow rates, while the flow rate is varied by adjusting the nozzle vane stagger angles. As shown in figure 15, with a range of 56.2% - 103.5% design flow (i.e. the stagger angle varies from 33° to 42°), static pressure at both side gaps inlet does not change evidently; at flow rates above 120% design flow (45°), the static pressure increases rapidly, and influence of main flow stream on the gap inlet flow increase. As mass flow rate increases, the impeller inlet static pressure, p_1 , increases leading to an increase in force F_1 and F_2 as indicated respectively by equation 6 and 7.

It is visible that inlet pressure of the back side gap is slightly larger than that of the front side gap, because the front side gap is connected to the outlet of the impeller in which the pressure is almost the lowest in the whole flow field, and the sealing effect of the front side gap is less well than that of the impeller back side gap.

Influence of Turbine Inlet Pressure

The liquid turbine can be operated at both design and off-design conditions, for example, the inlet pressure may vary, which can cause a change in the axial thrust. The influence of inlet pressure on axial thrust is also investigated numerically based on stage flow simulation at different inlet pressure.

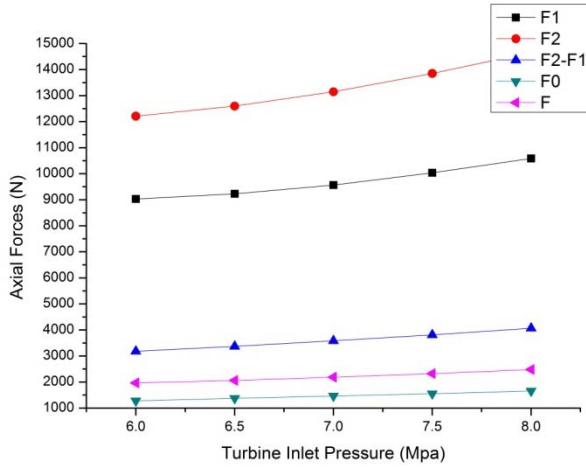


Figure 16 AXIAL THRUST COMPONENTS VARIATION AT DIFFERENT TURBINE INLET PRESSURE

As turbine inlet pressure increases, axial force F_0 and resultant force $F_2 - F_1$ increase as shown in figure 16, but the increase of resultant force $F_2 - F_1$ is larger than that of F_0 . The axial thrust is expressed by equation 1, i.e. $F = F_2 + F_4 - F_1 - F_0 - F_3$, where force F_3 and F_4 held constant as being described in section Axial Thrust Calculation. Based on the above analysis and equation 1, we can deduce that the axial thrust increases with turbine inlet pressure.

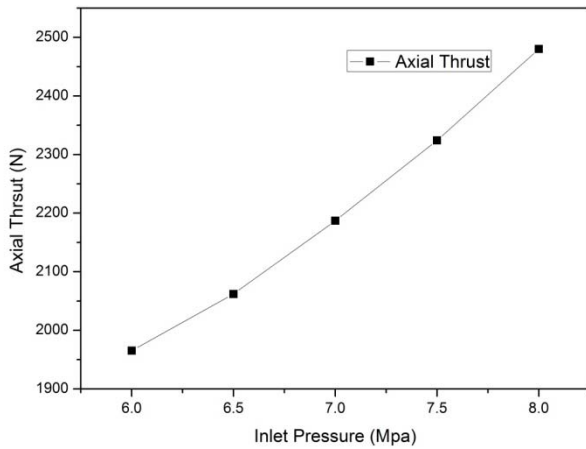


Figure 17 AXIAL THRUST WITH DIFFERENT INLET PRESSURES

As shown in figure 17, the axial thrust is increased from 1965.337 N to 2480.11 N, as the turbine inlet pressure varies from 6 Mpa to 8 Mpa. Such variation of axial thrust must be considered in the turbine design and operation.

Influence of Shaft Seal Clearance Size

To investigate the influence of geometric parameters on the axial thrust, parametric study was performed at design

condition for different shaft seal clearance size. Flow simulation is carried out in a turbine stage environment with the both front and back side impeller gaps.

For the operational turbine, due to mechanical wear, the tooth height of labyrinth seal will decrease with time, i.e. the gap between the tip of the labyrinth seal tooth and rotor will increase. This will influence the pressure distribution in the seal chamber and subsequently the axial thrust, which also need to be justified for safe operation.

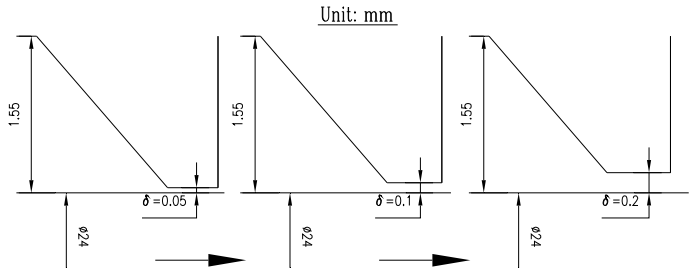


Figure 18 THE DIMENSION BETWEEN THE TOOTH AND THE ROTOR

As shown in the figure 18, the shaft seal clearance between the shaft seal tooth tip and the rotor, δ , is initially 0.05mm. To look at its influence on the impeller back side gap flow and rotor axial thrust, this seal clearance has been varied and four different sizes of seal clearance, 0.05mm, 0.1mm, 0.15mm, and 0.2mm, are used in the simulation. Figure 19 presents the predicted axial thrust versus the shaft seal clearance size. It is evident that the axial thrust decreases largely from 2187.021 to 352.093 N with an increase in the seal gap (δ). Figure 20 presents the static pressure variation of impeller back side surface along radial direction for different shaft seal clearances.

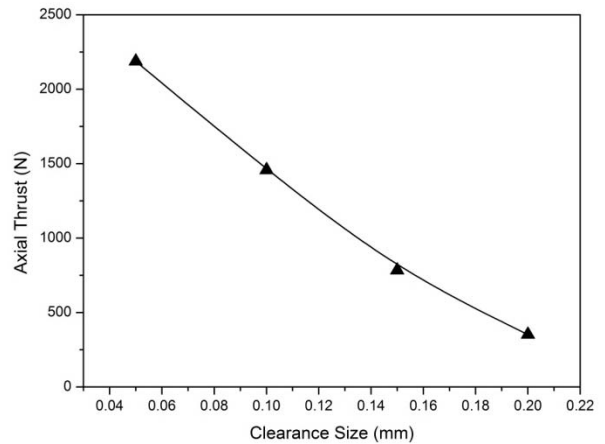


Figure 19 INFLUENCE OF SHAFT SEAL CLEARANCE ON AXIAL THRUST

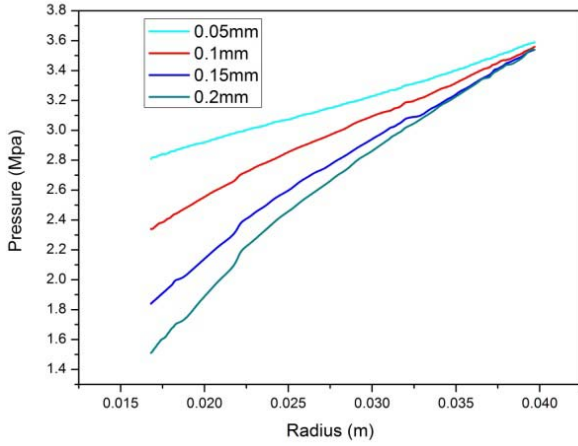


Figure 20 IMPELLER BACK SIDE GAP PRESSURE DISTRIBUTION VERSUS SHAFT SEAL CLEARANCE

As mentioned in the preceding context, the shaft seal chamber is connected to the impeller outlet, figure 1, thus the shaft seal outlet pressure is held as the turbine outlet pressure. Variation of the shaft seal clearance influences the main flow domain is small, thus the impeller back side gap inlet pressure almost remain unchanged, as shown in figure 20 by the right end points of the all curves. The reason for this may be that the back side gap inlet lies in the interface region of impeller main flow domain and back side gap small, and flow behavior in particular region is almost governed by the main flow stream, thus static pressure at the side gap inlet is held with the shaft clearance size. However, beyond this gap inlet region, influence of the main flow stream on gap flow behavior decreases gradually along the radial inward direction, and gap flow exhibits small clearance flow characteristics, that is, it largely depends on the size of shaft seal clearance, as shown in figure 20, pressure decreases with the shaft seal size at the same radial location. Consequently, the resultant pressure force, (i.e. F_2 as shown in figure 4) acting on the impeller back side surface become smaller, subsequently leading to evidently drop in the axial thrust.

4. EMPIRICAL METHOD

Numerical method permits sound prediction for axial thrust as detailed in the above context, but it is both time-consuming and costly, which requires a real environment 3-D flow simulation. The empirical methods are still in use simultaneously for a quick prediction of axial thrust. The empirical methods is analyzed and justified below by the comparison with the numerical one.

In the empirical method, the axial thrust is expressed by the same formula as introduced in section 2, and rewritten as

$$F = F_2 + F_4 - F_1 - F_0 - F_3$$

Where F_3 and F_4 are obtained by the same method as described in section 2, but F_1 , F_2 , and F_0 treated

empirically. Each component force of axial thrust have been shown in figure 4 in paragraph Axial Thrust Calculation.

In the empirical methods, to obtain the above mentioned three forces F_1 , F_2 , and F_0 , the following assumptions are used simultaneously [6, 7, 19]:

- (1) The angular velocity of flow in the impeller front and back side gaps is half of the rotor speed ($\omega_s = \omega / 2$);
- (2) Pressure in both front and back gaps is only dependent on the radius. Say the radial dimension in impeller front side gap is r_1 , and that in backside gap is r_2 , if $r_1 = r_2$, then pressure in both side gaps are equal, i.e.

$$P_{r1} = P_{r2}$$

- (3) The leakage flow through the impeller front side gap and shaft seals is neglected.

Clearly forces of F_1 and F_2 must be obtained based on the pressure distribution in the gaps and it is derived from the radial equilibrium condition.

As shown in figure 21, an elemental volume of flow in the gap is taken for analysis. Consider all the forces acting on this control volume, which includes the pressure forces acting on each control surface and centrifugal force as body force. It is noted that herein the gravitational force effect is neglected. Suppose all the forces are balanced along the radial direction, then we have

$$(p+dp)(r+dr)d\theta dz - prd\theta dz - 2(p+\frac{dp}{2})drdz \sin\frac{d\theta}{2} = \rho r dr d\theta dz \frac{c_u^2}{r} \quad (3)$$

It is reduced to

$$\frac{dp}{dr} = \frac{\rho c_u^2}{r} = \rho \omega_s^2 r \quad (4)$$

$$p_r = P_1 - \frac{\rho \omega^2}{32} (D_1^2 - D^2) \quad (5)$$

Where P_1 represents impeller inlet pressure, ρ is density and $D = 2r$.

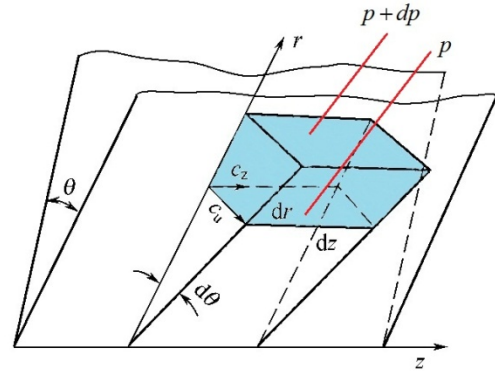


Figure 21 RADIAL EQUILIBRIUM CONDITION DIAGRAM

Based on the above analysis and assumptions, the axial

forces F_1 and F_2 can be obtained

$$F_2 = \int_{d_m/2}^{D_1/2} p_{r2} 2\pi r dr$$

$$= \frac{\pi}{4} (D_1^2 - d_m^2) P_1 - \frac{\pi \rho u_1^2}{32} [(D_1^2 - d_m^2) - \frac{(D_1^4 - d_m^4)}{2D_1^2}]$$
(6)

$$F_1 = \int_{D_2/2}^{D_1/2} p_{r1} 2\pi r dr$$

$$= \frac{\pi}{4} (D_1^2 - D_2^2) P_1 - \frac{\pi \rho u_1^2}{32} [(D_1^2 - D_2^2) - \frac{(D_1^4 - D_2^4)}{2D_1^2}]$$
(7)

To obtain F_0 , the momentum conservation equation is applied to the control volume between impeller inlet and outlet, then we have

$$F_0 = \frac{\pi}{4} (D_2'^2 - D_2^2) P_2 + q_m u_2$$
(8)

Additionally, F_3 and F_4 is obtained by

$$F_3 = \frac{D_2'^2 \pi P_2}{4} \quad \text{and} \quad F_4 = \frac{P_z \pi (d_m^2 - D^2)}{4}$$
(9)

Where P_2 represents the impeller outlet pressure, u_1 the impeller rim velocity, q_m the mass flow rate, u_2 the axial flow velocity at impeller outlet, and p_z the pressure in the shaft seal chamber.

With the above axial force components, the axial thrust can be readily calculated.

Table 3 COMPARISON WITH TWO METHODS

Axial Forces (N)	F_1	F_2	F_0	F_3	F_4	Axial thrust
Empirical	11541.51	13111.74	1386.56	162.77	216.12	237.02
Numerical	9562.71	13150.1	1465.6	162.77	216.12	2175.14

Table 3 compares the calculated axial thrust and forces by the numerical and empirical method. It is noted that for comparability between the two methods, the same impeller inlet and outlet pressure are used in the empirical calculations as the numerically predicted ones. The axial thrust by empirical method is 237.02 N, and by numerical method is 2175.14 N. Clearly there is considerable difference, and causes for this may be identified based on the comparisons of force component F_1 , F_2 and F_0 obtained by the two methods.

As shown in table 3, the empirical method predicts 11541 N for F_1 , and the numerical 9562 N, and a large difference is visible. Clearly the empirical method for predicting F_1 resulted from the front side gap flow is not reasonable. It is

clear also that two values, 13111 N and 13150 N, of F_2 are very closer, which demonstrates that the empirical formula as described by equation (6) for calculating the pressure force is fairly reasonable induced by the back side gap flow.

It is seen from the above comparison of F_1 and F_2 that both forces are induced by the side gap flows and predicted using the similar empirical formula (i.e. pressure in both gaps is assumed to be only dependent on the radius), but the results are very different. This may be associated with the different leakage flow characteristics in both gaps, because the geometry structures of the front side gap and back side gap are different, thus gap flow behaviour in both gaps is different. Thus, the gap flow induced force F_1 and F_2 must be quite different. If the same empirical formulas are used to predict these two forces, then different deviations would be produced.

As illustrated in figure 4, the seal chamber at the impeller back side is much longer than that at the front side, thus the leakage flow in the back side seal leakage chamber can be throttled more efficiently, thus the amount of the leakage flow rate is reduced to a minimum in CFD simulation; on the other hand, the empirical method also uses the “zero leakage flow” assumption as described the preceding paragraph, and influence of leakage flow is not considered in the empirical formulas. Clearly, the radial equilibrium condition with “zero leakage flow” assumptions is relatively suited for predicting the backside gap flow with longer throttling passage. Thus the predicted values of F_2 by the empirical method is closer to the numerical one in comparison with F_1 .

The empirical value of F_0 is 1386.56 N and somewhat smaller than the numerical one of 1465.6 N, but the difference is much small in comparison with F_1 . It may be concluded that F_0 may be evaluated without large error based on the integral form of momentum conservation equation, as given by equation 8.

From above analysis, it may be concluded that the empirical method permits quick prediction for the axial thrust, but it may also produce large error, which is mainly caused by the improper prediction of the axial force component acting on impeller induced by the impeller front side gap flow. To improve the accuracy of prediction, flow mechanism in the front side gap must be studied in depth to modify the empirical treatment for the gap flow.

5. CONCLUSIONS AND FUTURE WORK

A numerical model is established to simulate the turbine flow in a turbine stage environment, which includes the turbine main flow domain, impeller front and back side gaps, and shaft seal leakage. Flow behaviour in both main flow domain and impeller side gaps has been well exhibited by the numerical results. Influence on the axial thrust of different turbine operation conditions and shaft seal clearance are investigated respectively based on turbine stage flow simulation. An

empirical method is also used to predict the axial thrust and compared with the CFD based one. Conclusions arising from the present study are mainly the following:

- At the impeller back side gap inlet, the back flow is encountered even for design condition and it returns the impeller main flow stream; the impeller side gap flow has much influence on the axial thrust.
- The axial thrust increases as the inlet pressure increases and decreases as turbine flow rate increases.
- The axial thrust is influenced largely by the shaft seal clearance size and it decreases as the clearance grows.
- A large difference exists in the axial thrust calculated by the empirical method and CFD approach, and the reason is that axial force components caused by impeller main flow stream and its side gaps flow are approximated very roughly in the empirical method.

Future work will be conducted in several aspects. It is necessary to carry out the experiment study to validate the prediction of the axial thrust. Unsteady models with sliding mesh technique may be used to achieve a more accurate modeling of the flow physics and subsequent axial thrust prediction. The cavitation model should be incorporated into the CFD simulation to allow for the possible local evaporation of the liquefied gases.

6. ACKNOWLEDGEMENTS

The work is supported by the National 863 Plan of the Ministry of Science and Technology (Project No. 2007AA05Z202) and the National Natural Science Foundation of China under Grant 51006078(2010), and both are highly acknowledged by the authors.

7. NOMENCLATURE

q_m	mass flow rate (kg/s)
ω	angular velocity of the rotor (rad/s)
ω_s	angular velocity of the fluid in the gaps (rad/s)
p_r	pressure distribution in the gaps (Pa)
P_1	impeller inlet pressure (Pa)
P_2	impeller outlet pressure (Pa)
P_z	shaft seal chamber pressure (Pa)
u_1	rim velocity of the impeller (m/s)
u_2	axial velocity of impeller inlet (m/s)
F	axial thrust (N)
D	diameter (m)
ρ	density (kg / m^3)

REFERENCES

- [1] H Kimmel., 1997, "Speed controlled turbines for power recovery in cryogenic and chemical processing," World Pumps, 369, pp. 46-49.
- [2] Johnson, L L., Renaudin, Gerard., 1996, " Liquid Turbines Improve LNG Operations," Oil & Gas Journal, 94, pp. 31-36.
- [3] Sun Q.H., 2004, "Effect of an Expander with Overall Liquid on Efficiency of an Air Separation Process," Cryogenic Technology, No.3., pp. 17-19.
- [4] Franz R., Acosta A. J., Brennen C. E., Caughey T. K., 1990, "The Rotordynamic Forces on a Centrifugal Pump Impeller in the Presence of Cavitation", Journal of Fluids Engineering , ASME, Vol.112, pp.264-271
- [5] "Experimental evaluation of axial thrust in pumps", World Pumps, Vol. 393, June 1999, pp. 34-37.
- [6] Lobanoff, V. S., and Ross, R. R., 1985, Centrifugal Pumps Design & Application, Gulf Publishing Company, Houston.
- [7] Stepanoff, A. J., 1948, Centrifugal and Axial Flow Pumps, John Wiley & Sons, Inc., New York.
- [8] Kurokawa, J., Kamiyo, K., and Shimura, T., March-April 1994, "Axial Thrust Behavior in LOX-Pump of Rocket Engine", Journal of Propulsion and Power, 10, 2, pp. 244-250.
- [9] van Hooser, K., Bailey, J., and Majumdar, A., 1999, "Numerical Prediction of Transient Axial Thrust and Internal Flows in a Rocket Engine Turbopump," In 35th AIAA/ASME/SAE/ASEE Joint Propulsion Conference and Exhibit. AIAA Paper 99-2189.
- [10] Han, Z.X., Cizmas Paul G. A., 2001, "A CFD Method For Axial Thrust Load Prediction Of Centrifugal Compressors," ASME Paper No. GT2001-0568.
- [11] Della Gatta S., Salvadori S., Adami P., Bertolazzi L., 2006, "CFD Study For Assessment Of Axial Thrust Balance In Centrifugal Multistage Pumps,".
- [12] Gantar M., Florjancic D., Sirok B., 2002, "Hydraulic Axial Thrust in Multistage Pumps-Origins and Solutions," Fluids Eng. Trans. ASME , 124 (2), pp. 336-341.
- [13] Wen S.P., Yan H, Zhang C.H., 2004, "Calculation of Flow Field in Gap outside of Centrifugal Impeller," Fluid Machinery, No. 32(6), pp. 13-15.
- [14] Dorney, D. J., Bogdan Marcu, Ken Tran, Scott Sargent, 2003, "Calculation of Turbine Axial Thrust by Coupled CFD Simulation of the Main Flow Path and Secondary Cavity Flow in an SLI LOX Turbine," In 39th AIAA/ASME/SAE/ASEE Joint Propulsion Conference and Exhibit, AIAA 2003-4919.
- [15] Baumgarten S., Fritz J., Knierim C., Müller T., 2001, "Numerical Simulation of the Flow in a Boiler Circulating Pump," IMechE, Proc Instn Mech Engrs Vol 215, pp. 793-800.
- [16] Wang W.M., Gao J.J., Jiang Z.N., 2006, "Axial Thrust Research for High-pressure Centrifugal Compressor", Compressor Blower & Fan Technology, Vol. 6, pp. 1-4.
- [17] ANSYS ICEM 12.0 Help Manual
- [18] ANSYS CFX 12.0 Help Manual.
- [19] Huang Z.Y., Wang X.F., 2004, Turbocompressor, Chemical Industry Press, Beijing.